Inorganic Chemistry

Article

pubs.acs.org/IC

Diruthenium(III,III) Ethynyl-phenyleneimine Molecular Wires: Preparation via On-Complex Schiff Base Condensation

Steven P. Cummings, Zhi Cao, Phillip E. Fanwick, Anastasia Kharlamova, and Tong Ren*

Department of Chemistry, Purdue University, West Lafayette, Indiana 47907, United States

Supporting Information

ABSTRACT: The diruthenium compound *trans*-$Ru_2(DMBA)_4(C{\equiv}C{-}C_6H_4\text{-}4\text{-}CHO)_2$ (**1**; DMBA is *N,N′*-dimethylbenzamidinate) was prepared from the reaction between $Ru_2(DMBA)_4(NO_3)_2$ and $HC{\equiv}C{-}C_6H_4\text{-}4\text{-}CHO$ under the weak base conditions. The aldehyde groups of **1** undergo a condensation reaction with $NH_2C_6H_4\text{-}4\text{-}Y$ (Y = H and NH_2) to afford new compounds *trans*-$Ru_2(DMBA)_4(C{\equiv}C{-}C_6H_4\text{-}4\text{-}CH{=}N{-}C_6H_4\text{-}4'\text{-}Y)_2$ (Y = H (**2**) and NH_2 (**3**)). A related compound, $Ru_2(DMBA)_4(C{\equiv}C{-}C_6H_4\text{-}4\text{-}N{=}C(Me)Fc)_2$ (**4**), was also prepared from the reaction between $Ru_2(DMBA)_4(NO_3)_2$ and $HC{\equiv}C{-}C_6H_4{-}N{=}C(Me)Fc$. X-ray structural studies of compounds **1** and **2** revealed significant deviation from an idealized D_{4h} geometry in the coordination sphere of the Ru_2 core. Voltammetric measurements revealed four one electron redox processes for compounds **1**−**3**: the Ru_2 centered oxidation and reduction, and a pair of reductions of the imine or aldehyde groups. Compound **4** displays an additional oxidation attributed to the Fc groups. DFT calculations were performed on model compounds to gain a more thorough understanding of the interaction of the organic functional groups across the diruthenium bridge.

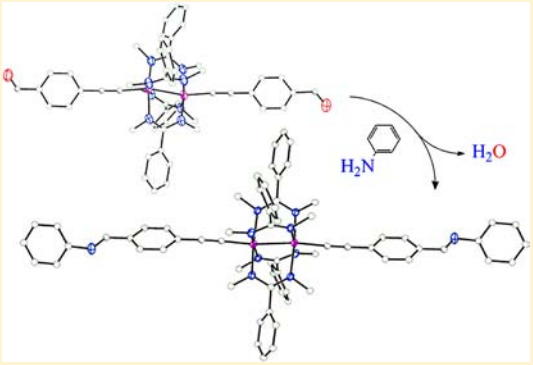

INTRODUCTION

For decades, metal alkynyl and alkenyl complexes have been investigated as building blocks for molecular wires,[1,2] nonlinear optical chromophores,[3] and photovoltaic materials.[4] Excellent charge transfer and molecular switching characteristics of molecular wires based on Fe,[5] Re,[6] Ru,[7] and Ru_2[8] compounds have been demonstrated through current−voltage (I−V) measurements at the single or few molecule level.[9] Among several types of diruthenium polyynyl and polyenyl compounds, those based on $Ru_2(DMBA)_4$ (DMBA is *N,N′*-dimethylbenzamidinate) are particularly attractive due to their rich and robust redox properties as well as the facile formation of bis-alkynyl adducts.[10,11] In contrast to the aforementioned successes based on polyynyl/polyenyl ligands, organometallic compounds containing heteroatoms in the conjugated pathway are far less common. Frisbie and co-workers recently reported that oligophenyleneimines (OPI) are efficient charge carriers in the donor−bridge−acceptor (D−B−A) scheme, revealing the potential of heteroatom bridges.[12,13] Charge transfer was found to proceed via a superexchange mechanism over short distances (up to 4 nm), and a hopping mechanism at extended distances (4−8 nm) with an exceptionally small attenuation constant (β) of 0.09 $Å^{-1}$ ($R = R_0e^{-\beta L}$; R and L are molecular resistance and length, respectively).[12] Accordingly, there is an interest in incorporating an OPI fragment into the conjugated backbone of $[M]{-}C{\equiv}C{-}R$, which may lead to interesting charge transfer characteristics. Further demonstration of the utility of phenyleneimine in molecular electronics came from the recent reports of Si nanogaps with organic molecular bridges by Ashwell et al.[14] The Si surface of the nanogap was first modified with 4-ethynylbenzaldehyde, which then underwent a Schiff base condensation reaction with an aromatic compound containing two terminal amino groups to complete the molecular bridge.

Transition-metal compounds with an imino-containing acetylide ligand are rare and limited to arylacetylides. As shown in Chart 1, these compounds can be classified as either the C-imino or N-imino type based on the imine orientation relative to the arylacetylene fragment. The N-imino type compounds of Ru(II), Au(I), and Ni(II) were prepared by Humphrey and co-workers from the dehydrohalogenation reactions between the imino-containing aryl acetylene and the appropriate Ru, Au, and Ni starting compounds.[15] In contrast, Lapinte and co-workers found that the (η^2-dppe)(η^5-Cp*)Fe based *N*-imino type compound can be obtained by an on-complex condensation reaction between (η^2-dppe)(η^5-Cp*)-$FeC{\equiv}C\text{-}4\text{-}(C_6H_4)NH_2$ and 2-pyridinecarboxaldehyde, while

Chart 1. Compounds with Imino-Containing Acetylide Ligands

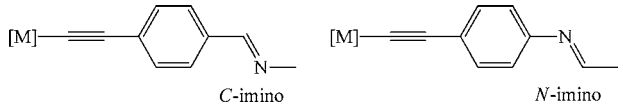

Received: January 24, 2012
Published: June 22, 2012

 © 2012 American Chemical Society

preparation via the dehydrohalogenation reaction failed.[16] Pt(II) based *C*-imino type compounds were also prepared from the condensation reaction between the aldehyde substituents of Pt-bound arylacetylides and aniline by Eisenberg and co-workers.[17] Previously, we reported the preparation of N-imino type $Ru_2(ap)_4$-compounds (*ap* = 2-anilinopyridinate) using the on-complex condensation reaction.[18] Described in this contribution are the preparation of *trans*-$Ru_2(DMBA)_4(C{\equiv}C{-}C_6H_4{-}4{-}CHO)_2$ (**1**), and subsequent synthesis of its derivatives **2** and **3** (Scheme 1) via condensation

Scheme 1. Synthesis of Ru_2(DMBA)-Alkynyls with Imine Substituent[a]

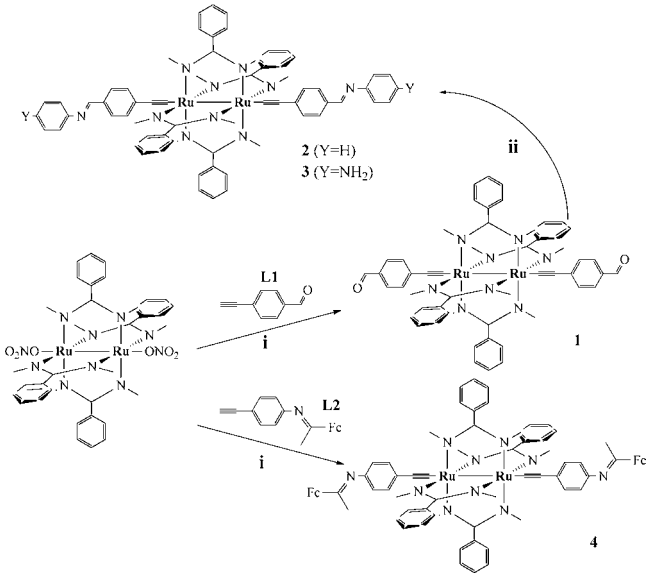

[a]Conditions: (i) $Ru_2(DBMA)_4(NO_3)_2$, $HNEt_2$; (ii) 4-Y-aniline, CF_3CO_2H/CH_3CO_2H.

with the appropriate arylamines. A related compound, $Ru_2(DMBA)_4(C{\equiv}C{-}C_6H_4{-}4{-}N{=}C(Me)Fc)_2$ (**4**), was prepared from the reaction between $Ru_2(DMBA)_4(NO_3)_2$ and $HC{\equiv}C{-}C_6H_4{-}N{=}C(Me)Fc$. While the synthesis of **1**−**3** is similar to that of $Ru_2(ap)_4$-based compounds, the resultant compounds are diamagnetic and of significantly different physical properties. Furthermore, the condensation reaction occurs simultaneously on both axial directions of $Ru_2(DMBA)_4$ core and hence permits faster extension than that of $Ru_2(ap)_4$-based compounds, where the extension is unidirectional. The impact of the imine moiety on the electronic structure of the diruthenium species was examined through structural, voltammetric, and computational studies.

■ RESULTS AND DISCUSSION

Synthesis. As a continuation of the study on peripheral modification of diruthenium paddlewheel species,[19] on-complex Schiff base condensations were previously carried out between the terminal amino group in $Ru_2(ap)_4(C{\equiv}C\text{-}3/4\text{-}C_6H_4{-}NH_2)$[20] and an arylaldehyde.[18] However, attempts to obtain an analogous $Ru_2(DMBA)_4(L_{ax})_2$ precursor, *trans*-$Ru_2(DMBA)_4(C{\equiv}C{-}C_6H_4{-}4{-}NH_2)_2$, from the reaction between $Ru_2(DMBA)_4(NO_3)_2$ and $4\text{-}HC{\equiv}C{-}C_6H_4{-}NH_2$ only led to intractable precipitates. Alternatively, the reaction between $Ru_2(DMBA)_4(NO_3)_2$ and 4-ethynylbenzaldehyde (**L1**, see Supporting Information) in the presence of diethylamine yielded compound **1** as shown in Scheme 1.[21] Both aldehyde groups of **1** undergo a simultaneous condensation reaction with aniline or *p*-phenylenediamine resulting in compounds **2** or **3**, respectively, with the *C*-imino linkage. To facilitate Schiff base condensation, both trifluoroacetic acid and acetic acid were tested as a Brønsted acid catalyst. The use of acetic acid allows for yields between 75 and 80% with a reaction time of ca. 3 h, while the use of trifluoroacetic acid led to significantly shortened reaction times (<5 min) and yields around 60 to 65% due to product degradation. As an oligomerization reaction between **1** and *p*-phenylenediamine could occur, a large excess of *p*-phenylenediamine was used to reduce the possibility of an oligomeric product. Compound **4** (Scheme 1) was prepared from the reaction between $Ru_2(DMBA)_4(NO_3)_2$ and $Fc\text{-}C(Me){=}N\text{-}4\text{-}C_6H_4{-}C{\equiv}CH$ (**L2**), the latter of which already contains a C-imino moiety, which will result in an N-imino Ru_2 product. The C-imino substitution in **2** and **3** has an electron withdrawing effect (σ_p = 0.42), while the N-imino substitution in **4** has an electron donating effect, and is described in more detail below. As the imine group in **4** was derived from an acetyl rather than aldehyde, this required the use of alumina to catalyze the reaction. The resulting imine potentially provides a more stable environment for the C═N bond by reducing the chance of hydrolysis; yet it should have minimal impact on the electronic structure.

Compounds **1**−**4** are all diamagnetic, and were readily characterized using ^1H NMR spectroscopy. Compound **1** has a distinct peak at 9.8 ppm that is indicative of an aldehyde, whereas the spectra of **2** and **3** feature a singlet at 8.3 ppm due to the methylidine proton of the imine group. FT-IR spectroscopy was useful in revealing product formation by the detection of an intense peak near 2050 cm^{-1} that is characteristic of the C≡C symmetric stretch in *trans*-$Ru_2(DMBA)_4$-acetylide compounds. A weak peak near 1619 cm^{-1} in compounds **2**, **3**, and **4** is attributed to the C═N stretch, while **1** has a strong peak at 1683 cm^{-1} indicative of a C═O stretch. Disappearance of the latter is an excellent indicator of the product purity for Schiff base condensation reactions.

Molecular Structures. Single crystals of **1** and **2** were grown via slow cooling of a THF:hexanes solution (1:5) and vapor diffusion of hexanes into a saturated THF solution, respectively. ORTEP plots of **1** and **2** are displayed in Figures 1 and 2, respectively, with selected bond lengths and angles given in Table 1. In both **1** and **2**, a crystallographic inversion center is present bisecting the Ru−Ru bond, and the asymmetric unit

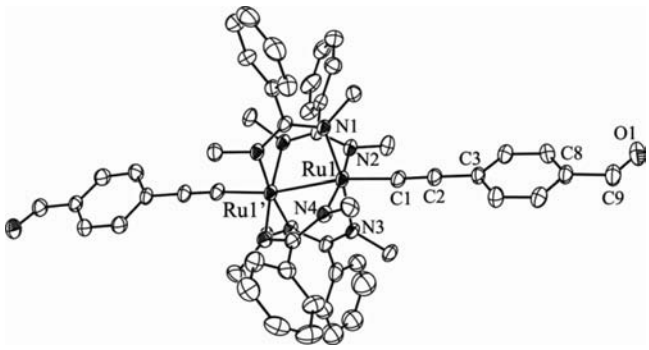

Figure 1. ORTEP plot of **1** at the 20% probability level. Hydrogen atoms were omitted for clarity.

dx.doi.org/10.1021/ic300182h | *Inorg. Chem.* 2012, 51, 7561−7568

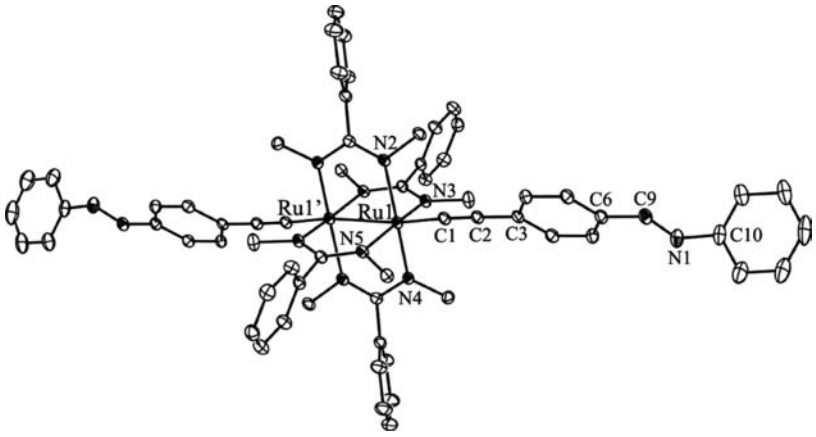

Figure 2. ORTEP plot of **2** at the 20% probability level. Hydrogen atoms were omitted for clarity.

Table 1. Selected Bond Lengths (Å) and Angles (deg) for 1 and 2

1		2	
Ru1−Ru1′	2.459(1)	Ru1−Ru1′	2.456(1)
Ru1−C1	1.970(7)	Ru1−C1	1.984(3)
Ru1−N1	2.051(5)	Ru1−N2	1.994(2)
Ru1−N2	2.142(5)	Ru1−N3	2.135(2)
Ru1−N3	2.038(5)	Ru1−N4	2.132(2)
Ru1−N4	1.981(6)	Ru1−N5	1.993(2)
C1−C2	1.22(1)	C1−C2	1.208(4)
C2−C3	1.44(1)	C2−C3	1.423(4)
C9−O1	1.22(1)	C9−N1	1.268(4)
		N1−C10	1.431(4)
Ru1−Ru1′−C1	163.8(2)	Ru1−Ru1′−C1	160.9(1)
Ru1−C1−C2	175.1(7)	Ru1−C1−C2	170.8(2)
C1−C2−C3	178.7(7)	C1−C2−C3	177.4(3)
C6−C9−O1	123.6(8)	C9−N1−C10	116.8(3)

contains one-half of the diruthenium molecule. The coordination sphere of $Ru_2(DMBA)_4$ in **1** and **2** are comparable to several previously reported $Ru_2(DMBA)_4(alkynyl)_2$ compounds.[22,23] The Ru−Ru bond lengths for **1** and **2** are in good agreement with *trans*-$Ru_2(DMBA)_4(C{\equiv}CPh{-}4{-}NO_2)_2$.[22,24] The observed elongation of the Ru−Ru bond is caused by the electron deficiency of the aldehyde and imine substituents, which further polarizes the Ru d_{z2} orbital toward C1.[11,22] A second-order Jahn−Teller distortion from a D_{4h} geometry is evident in the coordination sphere of the Ru_2 centers: (i) large variations among the Ru−N and Ru′−Ru−N bond lengths and angles, and (ii) the Ru−Ru−C angle being significantly bent from linear to 163.8 and 160.9° for **1** and **2**, respectively.[25,26] A detailed DFT study into the origin of the Ru−Ru−C bond angles deviation from linear for *trans*-$Ru_2(L)_4(C{\equiv}C{-}R)_2$ compounds resulted in an ideal angle of 158.7°,[27] which is exceptionally close to those obtained experimentally, especially for **2**.

The C9−N1 and C10−N1 bond lengths in **2** are consistent with lengths previously published for imino-phenylacetylides bound to ruthenium,[18] nickel,[28] platnium[17] and iron,[16] while the C9−N1−C10 bond angle (116.8°) is slightly smaller than other imino-phenylacetylide compounds which range from 119.1 to 121.7°. The imine bound aryl rings of **2** contain a significant dihedral angle (59.4°) around the imine moiety, of which is coplanar with the aryl-aldehyde derived phenyl.[17,28,29] The majority of secondary aldimine structures have a torsional angle between 29 and 41°, which is attributed primarily to a steric hindrance of the ortho hydrogen on the aniline ring and the methylidine hydrogen.[30] An evaluation of Humphery and co-workers' series of phenylacetylides on gold, nickel, and ruthenium containing isoelectronic -ene, -imine, and -azo linkers supports steric hindrance being a primary cause for the dihedral angle.[28,29] In general, the aryl rings linked by an -azo group tend to have smaller dihedral angles (4−20°), while the aryl linked -imine and -ene (*E* conformation) have increased torsional angles (8−50°). A packing diagram shows that the terminal aryl rings of two independent molecules of **2** are within 3.5 Å at their nearest point, signifying that this increase of the dihedral angle is electronic in origin and not due to π-interactions.

Electrochemistry. Previously reported *trans*-$Ru_2(DMBA)_4(C{\equiv}CR)_2$ compounds display one reversible oxidation (**A**, (III,III) to (III,IV)) and one reversible reduction (**B**, (III,III) to (III,II)) that are Ru_2 centered.[2,23,24,26,31−33] As described in Scheme 2 and Table 2, compounds **1**−**4** exhibit

Scheme 2. Redox Couple Assignments for Compounds 1−4

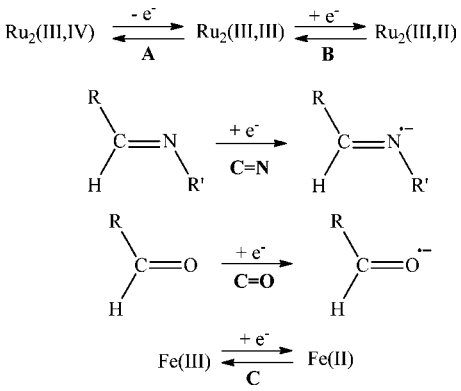

Table 2. Electrochemical Potentials (V, vs Ag/AgCl) of Compounds 1−4

	$E_{1/2}$ (C)	$E_{1/2}$ (A)	$E_{1/2}$ (B)	E_{pc} (C═N/O)[a]
1		0.609	−0.976	−1.860, −2.052
2		0.548	−1.017	−1.888, −1.986
3		0.545	−1.016	−1.815, −1.900
4	0.693	0.433	−1.140	−2.120

[a] E_{pc}(C═N/O) were obtained from DPV.

dx.doi.org/10.1021/ic300182h | Inorg. Chem. 2012, 51, 7561−7568

(Figure 3) analogous Ru_2 based redox couples. In addition, they display a second set of reductions which are assigned to the axial ligand functional groups (**C═O** and **C═N**). Compounds **3** and **4** display an additional $2e^-$ oxidation process, which is assigned to the simultaneous oxidation of the amino (**NH_2**) and ferrocenyl (**C**, Fc to Fc^+) groups, respectively. Few electrochemical studies have been carried out on imino-phenylacetylides bound to a transition metal, and to the best of our knowledge this marks the first one in which an imine orientation effect is studied.

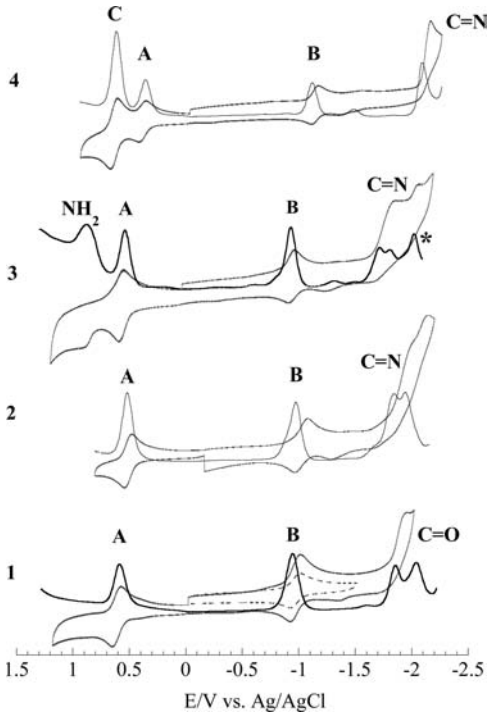

Figure 3. Cyclic and differential pulse voltammograms of **1**−**4**; * indicates degradation.

The first oxidations of **1**−**4** occur between 433 and 609 mV and are Ru_2-based for all compounds. Compound **1** is the most difficult to oxidize with the electrode potential being 60 mV higher than those of **2** and **3.** However, compound **4** is the easiest to oxidize with the electrode potential cathodically shifted by 176 mV from that of **1**. The first reduction of **1**−**4** is also Ru_2 centered, and its electrode potentials range from −0.976 to −1.140 V. The variation in reduction potentials follows the same trend as that of the oxidation with **4** being the most difficult to reduce and **1** being the easiest.

The changes in the Ru_2 redox potentials are in general accordance with the Hammett parameters of the substituents of arylacetylide ligands: **1** exhibits the most anodically shifted oxidation and reduction due to the aldehyde substituent being the strongest electron withdrawing group (σ_p = 0.42) among the compounds considered here.[34,35] $Ru_2(DMBA)_4$ bound to the C-imino moiety, as with **2** and **3**, displays similar oxidation and reduction potentials, as the 4-CH═N−C_6H_4−R is a substituent of comparable electron withdrawing ability (σ_p = 0.42) to an aldehyde. Although the C-imino and aldehyde groups have equivalent electron withdrawing strengths, there is a 60 mV difference in redox potentials, indicating that the substituent effect is not purely inductive. When the $Ru_2(DMBA)_4$ moiety is bound by an N-imino ligand, as with compound **4**, the Ru_2-based oxidation (**A**) and reduction couples (**B**) undergo a significant cathodic shift from those of compounds **1**−**3**, which is consistent with the strong electron donating nature of 4-N═CH−C_6H_4−R (σ_p = −0.55).[34] The strong electron donating effect of N-imino was also observed by both Lapinte and Shaabani,[16,36] where significant cathodic shifts of the Fe(II/III) couple were noticed when the amino precursor was converted to an *N*-imino substituent. It is also worth mentioning that the ferrocenyl group of **4** is C-imino bound and as a result the ferrocene/ferrocenium couple was observed at a potential 140 mV more positive than free ferrocene due to the *C*-imino group being an electron acceptor.

The cyclic voltammograms (CV) of compounds **1**−**4** display one or more $1e^-$ reductions from −1.80 to −2.10 V in addition to the Ru_2 centered couple (**B**). For **1**−**3**, the differential pulse voltammograms (DPV) clearly show two $1e^-$ reductions, while compound **4** has a single reduction peak that is greater than a one electron area. Previous studies in our lab have suggested this is a ligand based reduction.[18] It is well established that the imine and aldehyde groups are capable of being reduced, yet very little has been documented on their redox potentials when bound to metal centers. The cause of the variation in the imine reduction potentials is unclear, as evidenced by **3**, where **C═N** reduction couple is shifted positively when compared to that of **2**, despite the electron donating amino group which should increase the potential required for the imine reduction. One possible explanation, proposed in detail by Lapinte, is that an amino group in the para position is capable of manifesting a quinoidal resonance structure allowing for accommodation of the added electron.[37] According to the DPV for compounds **1**−**3**, the second reduction observed in CV occurs as two separate one-electron reductions. The stepwise reduction of two equivalent C═O (C═N) moieties may imply a long distance electronic coupling across the entire molecule, which was previously documented for the $Ru_2(DMBA)_4(C_{2n}Fc)_2$ type compounds.[23,31,38] Interestingly, in **4**, with the reversal of the imine group, this long distance coupling is not observed for either ferrocene or the imine group.

vis-NIR Electronic Spectroscopy. The vis-NIR spectra were recorded in THF for **1**−**4**. Compounds **1**−**4** have a low energy band with λ_{max}(nm) centered near 875 for **1**−**3** and 857 for **4** as shown in Figure 4. In the high energy region, compound **4** has a well-defined peak at 502 nm that is characteristic of $Ru_2(DMBA)_4(CCAr)_2$-type compounds.[22−24,31,33,39] Compounds **1**−**3**, however, exhibit an intense peak between 390 and 420 nm and a shoulder at 490 nm. The low energy transitions from 850 to 870 nm are ascribed to the HOMO−LUMO gap of a $\pi^*(Ru_2) \rightarrow \delta^*(Ru)_2$ and are in good agreement with the electrochemical gap of ca. 1.56 V obtained from cyclic voltammetry. This transition does have some axial ligand influence as seen with **4**, which is blue-shifted by 20 nm due to an increase in the antibonding overlap between π(C≡C) and $\pi^*(Ru_2)$ occurring from the electron donating character of the imine.[26,33] The well-defined high energy absorption band of **4** is tentatively assigned to a mixture of $\pi(N) \rightarrow \delta^*(Ru_2)$ and $\delta\ (Ru_2) \rightarrow \delta^*(Ru_2)$ transitions as in previous $Ru_2(DMBA)_4(C{\equiv}C{-}R)_2$ systems and corroborated by a previously published TD-DFT calculation.[23] The $\pi(N) \rightarrow \delta^*(Ru_2)/\delta\ (Ru_2) \rightarrow \delta^*(Ru_2)$ transition for **1**−**3** is overshadowed by a more intense and broad peak at ca. 400 nm, resulting in a shoulder at 490 nm that accounts for the orange-red color observed. The intense high energy transitions observed for **1**−**3** at 390 to 420 nm are likely a mixture of

dx.doi.org/10.1021/ic300182h | Inorg. Chem. 2012, 51, 7561−7568

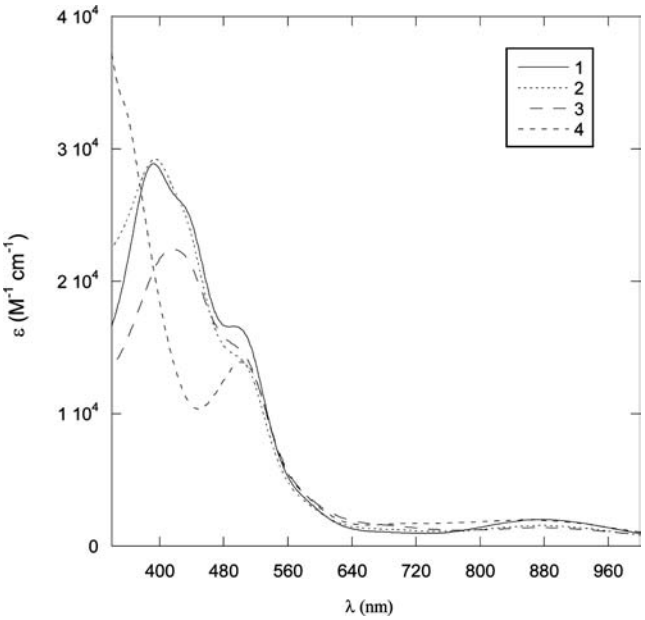

Figure 4. Vis-NIR spectra of **1**−**4** in THF.

ligand based $\pi \rightarrow \pi^*$ and MLCT transitions, similar to Pt-arylacetylide compounds bearing imino-substituents by Eisenberg.[17]

Density Functional Theory (DFT) Calculations. In an effort to better understand the unique electronic characteristics that these compounds display, spin-restricted DFT calculations were carried out for molecules **1** and **2** using optimized geometries based on the crystal structures without truncation. As electrochemistry revealed a significant difference in the ligand reduction in compounds **2**/**3** compared to that in **4**, a calculation of model **4′** was also carried out to determine if these differences were of an electronic origin. Model **4′** was built on the optimized structure of **2**, with the C═N bond being inverted to reflect the C-imino nature of **4** and the ferrocene group being replaced by the phenyl group to simplify calculations. DFT calculations were performed at the B3LYP/LanL2DZ level (by the Gaussian 03 suite).[40−42] For the purpose of comparison, a calculation consisting of polarization functions was carried out on **1** with the application of a 6-31G** basis set for H, C, N, and O, and a LanL2DZ(f) basis set for Ru resulting in **1′**.[43] Comparison of the calculations with and without polarization functions revealed no significant discrepancy. Hence, polarization functions were not applied for the remaining model calculations due to the significant increase in computation time considering the size of the system. The results of **1′** are detailed in the Supporting Information Table S1 and Figure S1. A qualitative discussion of the MO contribution is provided below, while a natural bond orbital (NBO) analysis for **1**, **2**, and **4′** was carried out with the percent contribution for distinct functional groups detailed in Table S2 of the Supporting Information.

The bond lengths of the optimized structures were in good agreement (Table S1 of the Supporting Information) with the crystal structures of **1** and **2**. The optimized Ru−Ru bond lengths (2.54−2.56 Å) are ca. 0.10 Å longer than the experimental bond lengths (2.46 Å), which is likely due to the underestimation of metal−metal interactions by the B3LYP method. The introduction of polarization functions does result in a slightly improved bond length of 2.52 Å.[23] It is worth noting that previous DFT calculations had put the Ru−Ru bond length between 2.61 and 2.65 Å using calculations without polarization, but based on a truncated DMBA ligand model.[27,39] The bond angles of **1** and **2** are also in good agreement with experimental values, except for the Ru1−C1−C2 and C9−N1−C10 of **2** where C9−N1−C10 increases from 116.8 to 122° putting the nitrogen in a more trigonal planar orientation. The Ru1−C1−C2 angle of **2** was 175°, which is a 5° increase from the experimental value.

Since the DFT results for **1**, **2**, and **4′** are quite similar, the valence MOs of **1** are discussed in detail with the contour plots and energy levels shown in Figure 5. Contour plots of the

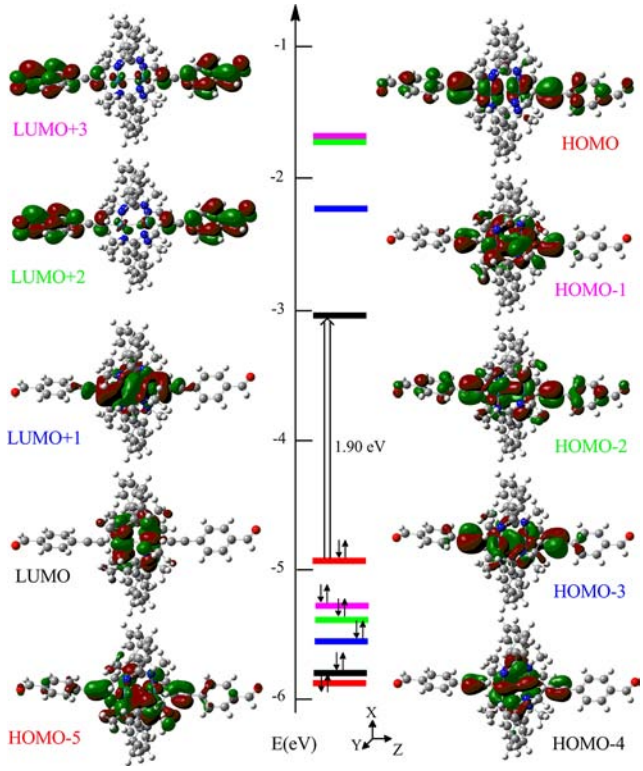

Figure 5. MO diagram of **1** based on spin-restricted DFT calculations.

valence MOs for **2** and **4′** can be found in the Supporting Information as Figures S2 and S3, respectively. The HOMO of **1** is an antibonding combination of π_{xz}*(Ru−Ru) and π(C≡C) with some contribution from the imine/aldehyde moiety, while the HOMO-1 is an antibonding combination of the π_{xz}(Ru−Ru) and π(C≡C). The HOMO-2 of **1** is an antibonding combination of π(C≡C) and π_{xz}(Ru−Ru) with additional contribution from π*(aryl), while the contribution from π_{xz}(Ru−Ru) decreases slightly in **2** and **4′**. Although the HOMO-3 is formally an antibonding combination of π_{yz}*(Ru−Ru) and π(C≡C), there is a significant σ-type overlap between two d_{yz} orbitals due to the distortion of the Ru_2 coordination sphere, which results in a partial σ-bond between two Ru centers.[39] The HOMO-4 is δ(Ru−Ru), though only weak orbital overlap is present, due to the small underestimation of the metal−metal interaction in conjunction with distortion of the coordination sphere. On the basis of formal molecular orbital assignments of the HOMO to the HOMO-4, the ground state electronic configuration is $\pi^4\delta^2\pi^{*4}$, which is in agreement with previous studies of *trans*-Ru_2(III,III)$(L_{ax})_2$ type compounds.[23,27] The LUMO and LUMO+1 are primarily

metal in character being the δ^*(Ru−Ru) and σ^*(Ru−C) orbitals, respectively. The LUMO+2 and LUMO+3 are primarily the antibonding interactions between π (aldehyde/imine) and π (aryl) orbitals of the ligand with a minimal presence of π_{yz} and π_{yz}^*(Ru−Ru). The HOMO-5 is mostly made of the π(N) of the amidinate ligands with a modest contribution with the π_{yz}(Ru−Ru) and π(C≡C).

The HOMO of **1** (−4.92 eV) is the lowest in energy with **4′** being the highest (−4.57 eV) and **2** in-between at −4.73 eV. This energetic order is consistent with electrochemical results, where the one electron-oxidation of **2** is easier than that of **1** but more difficult than **4**. The same trend holds true for the LUMO energies of **1**, **2**, and **4′**, which correlate well with the reduction potentials of the Ru_2(III,III) to Ru_2(III,II) couple. The reduction of **1** is the easiest as well as having the lowest lying LUMO at −3.02 eV followed by **2** and **4′** with the LUMO occurring at −2.75 and −2.64 eV, respectively. The HOMO−LUMO gaps of **1**, **2**, and **4′** are 1.90, 1.98, and 1.93 eV, respectively, and are in good agreement with the energy gaps previously calculated for *trans*-$Ru_2(DMBA)_4(C{\equiv}C{-}R)_2$ models.[23,39] The LUMO+2 and LUMO+3 for **1** and **2** are separated by 0.03 eV, while in **4′** these orbitals are degenerate.

In order to understand the change in the electronic structure for $Ru_2(DMBA)_4$ upon a one electron reduction, a spin-unrestricted DFT calculation was performed for $(\mathbf{2})^-$ which is a Ru_2(III,II) species adapted from the optimized structure of **2**. The calculation was carried out with $S = 1/2$, which provided a molecular geometry (Table S1 of the Supporting Information) and occupied molecular orbitals not too dissimilar to that of the neutral species. Upon reduction, the LUMO in **2** becomes the SOMO of $(\mathbf{2})^-$ as shown in Figure 6. The most marked difference upon reduction is an increase in the Ru−Ru and Ru−N bond lengths, due to the increased electron density on the Ru_2 core. The LUMO+1 of **2** is significantly destabilized, becoming the LUMO+2 for $(\mathbf{2})^-$, while the LUMO+2 and LUMO+3 of **2** become the LUMO and LUMO+1 in $(\mathbf{2})^-$. This gives support to the stepwise reduction of the organic functional group occurring before a second Ru_2 centered reduction. There is a slight but significant increase in the contribution of the $\pi_{xz}^*(Ru_2)$ in the LUMO and LUMO+1 of $(\mathbf{2})^-$, providing support for a superexchange pathway for electronic coupling between of the redox active C═O/C═N groups.

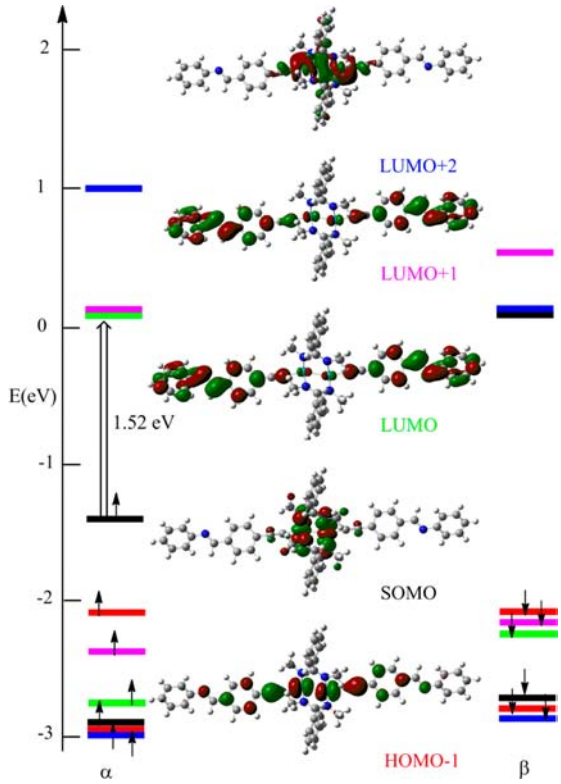

Figure 6. MO diagram of model compound $(\mathbf{2})^-$ based on spin-unrestricted DFT calculations; The α spin Kohn−Sham orbitals are shown with energy levels for both spins.

■ CONCLUSIONS

The on-complex Schiff base condensation has been successfully expanded from a monoadduct to a bis-adduct phenylimine system using Ru_2(III,III) increasing the scope of peripheral covalent modification chemistry.[19] Electronic interactions between distant organic aldehyde/imine groups in compounds **1**−**3** was inferred from electrochemical data and rationalized with the aid of DFT calculations. While the ligand centered mixed valency was not probed due to highly cathodic reduction potential in this contribution, it is worth noting that ligand-based mixed valency has been confirmed in other dinuclear systems by Chisholm and co-workers.[44] Work is continuing with **1** and **3** to form a monolayer covalently bound to a silicon surface in order to interrogate the electronic interactions of diruthenium and the silicon surface.

■ EXPERIMENTAL SECTION

General. 4-Bromobenzaldehyde, 4-iodoaniline, aniline, and *p*-phenylenediamine were purchased from Sigma-Aldrich, trimethylsilylacetylene was purchased from GFS chemicals, and acetylferrocene was purchased from STREM chemicals. $Ru_2(DMBA)_4(NO_3)_2$ was synthesized according to a literature procedure.[21] Toluene and diethylamine were distilled over CaH_2; THF was distilled over Na/benzophenone. Phenylenediamine was recrystallized from EtOH and all other reagents were used as received. The synthesis and characterization of 4-ethynylbenzaldehyde (**L1**) and $Fe(\eta^5C_5H_5)$-$(\eta^5C_5H_4{-}C(Me){=}N{-}4{-}Ph{-}C{\equiv}C{-}H)$ (**L2**) can be found in the Supporting Information. Syntheses were carried out using standard Schlenk techniques unless noted otherwise and were monitored by TLC using 3:7 EtOAc:hexanes for all reactions unless otherwise stated. ^{1}H NMR spectra were obtained using a Varian 300 MHz in $CDCl_3$. UV−vis-NIR was collected on a JASCO V-670 spectrophotometer in THF. Infrared spectra were collected on a JASCO FT-IR 6300 spectrometer via ATR on a ZnSe crystal. HR-nESI-MS spectra were performed on a QqQ tandem mass spectrometer in CH_2Cl_2 (QSTAR XL; Applied Biosystems/MDS Sciex, Concord, ON, Canada). Cyclic voltammograms were recorded in a 0.2 M *n*-Bu_4PF_6 and 1.0 mM diruthenium compound solution in N_2 degassed THF by a CHI620A voltammetric analyzer using a glassy carbon electrode (diameter = 2 mm), Pt-wire counter electrode, and a Ag/AgCl reference electrode using ferrocene as an internal reference (corrected to 0.565 V for **1** and **2**).

Attempted Synthesis of *trans*-$Ru_2(DMBA)_4(C{\equiv}C{-}C_6H_4{-}4{-}NH_2)_2$. A 25 mL Schlenk flask containing 0.055 mmol $Ru_2(DMBA)_4(NO_3)_2$ and 0.55 mmol 4-ethynylaniline was thoroughly degassed, to which was added 20 mL THF and 1 mL $HNEt_2$. The solution slowly became yellow-brown in color resulting in a baseline product according to TLC (3:7 EtOAc:hex). No red product was ever detected by TLC and the solid product isolated was soluble in common organic solvents, which made characterization difficult.

***trans*-$Ru_2(DMBA)_4(C{\equiv}C{-}4{-}Ph{-}CHO)_2$ (1).** To a 50 mL Schlenk flask with 0.295 mmol $Ru_2(DMBA)_4(NO_3)_2$ and 0.87 mmol 4-ethynylbenzaldehyde was added 20 mL THF and 3 mL $HNEt_2$; the

solution became orange-red over several hours. The solution was filtered through a diatomaceous earth plug and the solvents were removed on rotovap. Compound **1** was isolated as an orange-red solid (0.256 mmol, 87%) after being recrystallizied from THF/hexanes. Data for **1**: R_f = 0.55; ^{1}H NMR: 3.29 (*s* − 24H, CH_3), 7.03 (*d* − 8H, aromatic), 7.12 (*d* − 4H, aromatic), 7.45 (*d* − 12 H, aromatic), 7.67 (*d* − 4H, aromatic), 9.84 (*s* − 2H, C*H*═O); nESI-HR-MS, $[M+H]^+$ − 1050.248, (calc. 1050.212); visible spectra, λ_{max} (nm, ε (M^{-1} cm^{-1}): 877(2000), 495(16000); IR (cm^{-1}): C≡C − 2053 (s), C═O − 1683(s); Electrochemistry ($E_{1/2}$, V; ΔE_p; $i_{backward/forward}$): **A**, 0.609, 0.039, 0.98; **B**, −0.976, 0.049, 0.86; **C═O** (based on DPV) −1.860, −2.052.

***trans*-Ru$_2$(DMBA)$_4$(C≡C−4-Ph−CH═N−Ph)$_2$ (2).** A 50 mL Schlenk flask was charged with 0.082 mmol **1**, 0.15 mmol aniline, 30 mL dry-THF and 10 mL EtOH. To the solution was added 2 drops of acetic acid, and the reaction was monitored by TLC using 1:3 THF:hexanes. Upon completion, the reaction mixture was filtered through a deactivated silica plug and the solvents were removed under reduced pressure. The solid residue was recrystallized in THF:MeOH to yield 0.062 mmol purple solid (76% based on Ru). Alternatively, the reaction was performed in THF using trifluoroacetic acid with a yield of ca. 65%, but with a significantly shortened reaction time. Data for **2**: R_f = 0.60; ^{1}H NMR: 3.31 (*s* − 24H, CH_3), 7.03 (*d* − 8H, aromatic), 7.17 (*t* − 12H, aromatic), 7.41 (*m* − 14H, aromatic), 7.71 (*d* − 4H, aromatic), 8.34 (*s* − 2H, C*H*═N); nESI−HR−MS, $[M+H]^+$ − 1200.344, (calc. 1200.433); visible spectra, λ_{max} (nm, ε (M^{-1} cm^{-1}): 492(14000), 875(1500); IR (cm^{-1}): C≡C − 2065(s), C═N − 1619(w); Electrochemistry ($E_{1/2}$, V; ΔE_p; $i_{backward/forward}$): **A**, 0.548, 0.032, 0.88; **B**, −1.017, 0.034, 1.00; E_{pc}: **C═N** (based on DPV), −1.888, −1.986.

***trans*-Ru$_2$(DMBA)$_4$-(C≡C−4-Ph−CH═N−4′-Ph−NH$_2$)$_2$ (3).** Using the same procedure as **2** with trifluoroacetic acid, 0.508 mmol **1** and 3.28 mmol *p*-phenylenediamine were reacted to yield 0.339 mmol purple solid (67% based on Ru). Data for **3**: R_f = 0.1 (THF:hexanes, 1:1); ^{1}H NMR: 3.31 (*s* − 24H, CH_3), 4.03 (*s* − 4H, NH_2), 6.70 (*d* − 4H, aromatic), 7.01 (*d* − 4H, aromatic), 7.08 (*d* − 6H, aromatic), 7.15 (*d* − 6H, aromatic), 7.46 (*d* − 12H, aromatic), 7.70 (*d* − 4H, aromatic), 8.30 (*s* − 2H, C*H*═N); nESI−HR−MS, $[M+2H]^{+2}$ − 615.661, (calc. 615.733), $[M+H]^+$ − 1230.369, (calc. 1230.456); visible spectra, λ_{max} (nm, ε (M^{-1} cm^{-1}): 492(14000), 871(1400); IR (cm^{-1}): NH_2 − 3450, 3378, 3318(m), C≡C − 2071(s), C═N − 1619(w); Electrochemistry ($E_{1/2}$, V; ΔE_p; $i_{backward/forward}$): E_{pa}: **NH$_2$**, 0.888; **A**, 0.545, 0.030, 0.80; **B**, −1.016, 0.031, 1.00; E_{pc}: **C═N** (based on DPV), −1.815, −1.900.

***trans*-Ru$_2$(DMBA)$_4$-[(C≡C−4-Ph−N═C(Me)-η^5C$_5$H$_4$)(η^5C$_5$H$_5$)-Fe]$_2$ (4).** Following the procedure for the synthesis of **1**, 0.086 mmol **L2** was reacted with 0.046 mmol Ru$_2$(DMBA)$_4$(NO$_3$)$_2$. Upon completion, the reaction mixture was filtered and recrystallized in EtOAc:hexanes to yield 0.026 mmol (62%, based on Fe). Data for **4**: R_f = 0.40; ^{1}H NMR using C_6D_6: 1.845 (*s* − 6H, CH_3), 3.288 (*s* − 24H, CH_3), 3.967 (*s* − 10H, Cp*), 4.146 (*s* − 4H, Cp*), 4.584 (*s* − 4H, Cp*), 6.534 (*d* − 4H, aromatic), 6.909 (*d* − 8H, aromatic), 7.053 (*d* − 8H, aromatic), 7.233 (*d* − 8H, aromatic), nESI−HR−MS, $[M+H]^+$ − 1444.309, (calc. 1444.329); visible spectra, λ_{max} (nm, ε (M^{-1} cm^{-1}): 502(14000), 707(1700), 858(2000); IR (cm^{-1}): C≡C − 2078(s), C═N − 1621(s); Electrochemistry ($E_{1/2}$, V; ΔE_p; $i_{backward/forward}$): **A**, 0.433, 0.030, 0.63; **C**, 0.693, 0.030, 0.87; **B**, −1.140, 0.032, 0.68; E_{pc} (based on DPV), **C═N**, −2.120.

X-ray Data Collection, Processing, And Structure Analysis and Refinement for Crystal. Preliminary examination and data collection were performed on a Rigaku Rapid II image plate diffractometer with CuKα radiation (λ = 1.5418 Å) and the structures were solved using the structure solution program PATTY in DIRDIF99,[45] and refined using SHELX-07.[46] Cell constants for data collection were obtained from least-squares refinement, using the setting angles of 9536 reflections in the range of 2 < θ < 72° for **1** and 5815 reflections in the range 3 < θ < 72° for **2**. Crystal data for **1**: $C_{54}H_{49}N_8O_2Ru_2\cdot(C_4H_8O)_2$, FW = 1188.40, monoclinic, *C*2/*c*, *a* = 21.142(1), *b* = 17.907(1), *c* = 16.4044(7) Å, β = 115.188(4)°, V = 5618.0(6) Å^3, *Z* = 4, $D_{calc.}$ = 1.405 g cm^{-1}, *R1* = 0.059, *wR2* = 0.163. Crystal data for **2**: $C_{66}H_{64}N_{10}Ru_2$, FW = 1199.45, monoclinic, *C*2/*c*, *a* = 18.5186(7), *b* = 11.3288(4), *c* = 29.7899(9) Å, β = 104.300(3)°, V = 6056.1(4) Å^3, *Z* = 4, $D_{calc.}$ = 1.315 g cm^{-1}, *R1* = 0.034, *wR2* = 0.083.

Computational Methods. The full geometry optimizations of structures **1** and **2** were based on obtained crystal structures of **1** and **2** using the density functional theory (DFT) method,[47] which was based on the hybrid B3LYP[40] density functional model. The basis set used for all atoms was the LanL2DZ[48] and considered the involvement of metals. All calculations were carried out with the Gaussian 03 suite programs.[42]

■ ASSOCIATED CONTENT

Supporting Information

Experimental for **L1**, **L2**, and DFT details of model compounds **1**, **1′**, **2**, **4′**, and (**2**)$^-$. X-ray crystallographic details (CIF) of **1** and **2**. This material is available free of charge via the Internet at http://pubs.acs.org.

■ AUTHOR INFORMATION

Corresponding Author

* Phone. (765) 494-5466. Fax: (765) 494-0239. E-mail: tren@purdue.edu.

Notes

The authors declare no competing financial interest.

■ ACKNOWLEDGMENTS

We gratefully acknowledge financial support from both the National Science Foundation (CHE 1057621) and Purdue Research Foundation (fellowship to Z.C.).

■ REFERENCES

(1) Nast, R. *Coord. Chem. Rev.* **1982**, *47*, 89−124. Hagihara, N.; Sonogashira, K.; Takahashi, S. *Adv. Polym. Sci.* **1981**, *41*, 149−179. Manna, J.; John, K. D.; Hopkins, M. D. *Adv. Organomet. Chem.* **1995**, *38*, 79−154. Paul, F.; Lapinte, C. *Coord. Chem. Rev.* **1998**, *178−180*, 431−509. Higgins, S. J.; Nichols, R. J.; Martin, S.; Cea, P.; Zant, H. S. J. v. d.; Richter, M. M.; Low, P. J. *Organometallics* **2011**, *30*, 7−12. Costuas, K.; Rigaut, S. *Dalton Trans.* **2011**, *40*, 5643−5658.

(2) Ren, T. *Organometallics* **2005**, *24*, 4854−4870.

(3) Whittall, I. R.; McDonagh, A. M.; Humphrey, M. G.; Samoc, M. *Adv. Organomet. Chem.* **1998**, *42*, 291−362. Zhou, G.-J.; Wong, W.-Y. *Chem. Soc. Rev.* **2011**, *40*, 2541−2566.

(4) Wong, W.-Y.; Ho, C.-L. *Acc. Chem. Res.* **2010**, *43*, 1246−1256.

(5) Le Narvor, N.; Toupet, L.; Lapinte, C. *J. Am. Chem. Soc.* **1995**, *117*, 7129−7138. Tanaka, Y.; Shaw-Taberlet, J. A.; Justaud, F.; Cador, O.; Roisnel, T.; Akita, M.; Hamon, J.-R.; Lapinte, C. *Organometallics* **2009**, *28*, 4656−4669. Hoffert, W. A.; Rappé, A. K.; Shores, M. P. *J. Am. Chem. Soc.* **2011**, *133*, 20823−20836.

(6) Weng, W.; Ramsden, J. A.; Arif, A. M.; Gladysz, J. A. *J. Am. Chem. Soc.* **1993**, *115*, 3824−3825. Dembinski, R.; Bartik, T.; Bartik, B.; Jaeger, M.; Gladysz, J. A. *J. Am. Chem. Soc.* **2000**, *122*, 810−822.

(7) Bruce, M. I.; Low, P. J.; Costuas, K.; Halet, J.-F.; Best, S. P.; Heath, G. A. *J. Am. Chem. Soc.* **2000**, *122*, 1949−1962. Hamon, P.; Justaud, F.; Cador, O.; Hapiot, P.; Rigaut, S.; Toupet, L.; Ouahab, L.; Stueger, H.; Hamon, J.-R.; Lapinte, C. *J. Am. Chem. Soc.* **2008**, *130*, 17372−17383. Olivier, C.; Costuas, K.; Choua, S.; Maurel, V.; Turek, P.; Saillard, J.-Y.; Touchard, D.; Rigaut, S. *J. Am. Chem. Soc.* **2010**, *132*, 5638−5651. Li, F.; Cheng, J.; Chai, X.; Jin, S.; Wu, X.; Yu, G.-A.; Liu, S. H.; Chen, G. Z. *Organometallics* **2011**, *30*, 1830−1837. Fox, M. A.; Guennic, B. L.; Roberts, R. L.; Brue, D. A.; Yufit, D. S.; Howard, J. A. K.; Manca, G.; Halet, J.-F.; Hartl, F. e.; Low, P. J. *J. Am. Chem. Soc.* **2011**, *133*, 18433−18446.

(8) Xu, G.-L.; Zou, G.; Ni, Y.-H.; DeRosa, M. C.; Crutchley, R. J.; Ren, T. *J. Am. Chem. Soc.* **2003**, *125*, 10057−10065. Ying, J.-W.; Liu, I. P.-C.; Xi, B.; Song, Y.; Campana, C.; Zuo, J.-L.; Ren, T. *Angew. Chem., Int. Ed.* **2010**, *49*, 954−957. Xi, B.; Liu, I. P. C.; Xu, G.-L.; Choudhuri,

M. M. R.; DeRosa, M. C.; Crutchley, R. J.; Ren, T. *J. Am. Chem. Soc.* **2011**, *133*, 15094−15104.
(9) Blum, A. S.; Ren, T.; Parish, D. A.; Trammell, S. A.; Moore, M. H.; Kushmerick, J. G.; Xu, G. L.; Deschamps, J. R.; Pollack, S. K.; Shashidhar, R. *J. Am. Chem. Soc.* **2005**, *127*, 10010−10011. Kim, B.; Beebe, J. M.; Olivier, C.; Rigaut, S.; Touchard, D.; Kushmerick, J. G.; Zhu, X.-Y.; Frisbie, C. D. *J. Phys. Chem. C.* **2007**, *111*, 7521−7526. Mahapatro, A. K.; Ying, J.; Ren, T.; Janes, D. B. *Nano Lett.* **2008**, *8*, 2131−2136. Luo, L.; Benameur, A.; Brignou, P.; Choi, S. H.; Rigaut, S.; Frisbie, C. D. *J. Phys. Chem. C.* **2011**, *115*, 19955−19961. Ballmann, S.; Hieringer, W.; Secker, D.; Zheng, Q.; Gladysz, J. A.; Görling, A.; Weber, H. B. *ChemPhysChem.* **2011**, *11*, 2256−2260. Benameur, A.; Brignou, P.; Piazza, E. D.; Hervault, Y.-M.; Norel, L.; Rigaut, S. *New J. Chem.* **2011**, *35*, 2105−2113.
(10) Xu, G. L.; Campana, C.; Ren, T. *Inorg. Chem.* **2002**, *41*, 3521−3527. Xi, B.; Ren, T. *C. R. Chimie.* **2009**, *12*, 321−331.
(11) Ren, T.; Xu, G. L. *Commun. Inorg. Chem.* **2002**, *23*, 355−380.
(12) Choi, S. H.; Kim, B.; Frisbie, C. D. *Science* **2008**, *320*, 1482−1486.
(13) Choi, S. H.; Risko, C.; Delgado, M. C. R.; Kim, B.; BreÌdas, J.-L.; Frisbie, C. D. *J. Am. Chem. Soc.* **2010**, *132*, 4358−4368.
(14) Ashwell, G. J.; Phillips, L. J.; Robinson, B. J.; Urasinska-Wojcik, B.; Lambert, C. J.; Grace, I. M.; Bryce, M. R.; Jitchati, R.; Tavasli, M.; Cox, T. I.; Sage, I. C.; Tuffin, R. P.; Ray, S. *ACS Nano* **2010**, *4*, 7401−7406. Ashwell, G. J.; Phillips, L. J.; Robinson, B. J.; Barnes, S. A.; Williams, A. T.; Urasinska-Wojcik, B.; Lambert, C. J.; Grace, I. M.; Cox, T. I.; Sage, I. C. *Angew. Chem., Int. Ed.* **2011**, *50*, 8722−8726.
(15) Whittall, I. R.; Humphrey, M. G.; Houbrechts, S.; Persoons, A.; Hockless, D. C. R. *Organometallics* **1996**, *15*, 5738−5745. Whittall, I. R.; Cifuentes, M. P.; Humphrey, M. G.; Luther-Davies, B.; Samoc, M.; Houbrechts, S.; Persoons, A.; Heath, G. A.; Bogsanyi, D. *Organometallics* **1997**, *16*, 2631−2637. Whittall, I. R.; Humphrey, M. G.; Persoons, A.; Houbrechts, S. *Organometallics* **1996**, *15*, 1935−1941.
(16) Ghazala, S. I.; Gauthier, N.; Paul, F.; Toupet, L.; Lapinte, C. *Organometallics* **2007**, *26*, 2308−2317.
(17) Wadas, T. J.; Chakraborty, S.; Lachicotte, R. J.; Wang, Q.-M.; Eisenberg, R. *Inorg. Chem.* **2005**, *44*, 2628−2638.
(18) Cummings, S. P.; Geanes, A. R.; Fanwick, P. E.; Kharlamova, A.; Ren, T. *J. Organomet. Chem.* **2011**, *696*, 3955−3960.
(19) Ren, T. *Chem. Rev.* **2008**, *108*, 4185−4207. Ren, T. *C. R. Chim.* **2008**, *11*, 684−692.
(20) Cummings, S. P.; Cao, Z.; Liskey, C. W.; Geanes, A. R.; Fanwick, P. E.; Hassell, K. M.; Ren, T. *Organometallics* **2010**, *29*, 2783−2788.
(21) Xu, G. L.; Jablonski, C. G.; Ren, T. *Inorg. Chim. Acta* **2003**, *343*, 387−390.
(22) Hurst, S. K.; Xu, G. L.; Ren, T. *Organometallics* **2003**, *22*, 4118−4123.
(23) Xu, G. L.; Crutchley, R. J.; DeRosa, M. C.; Pan, Q. J.; Zhang, H. X.; Wang, X. P.; Ren, T. *J. Am. Chem. Soc.* **2005**, *127*, 13354−13363.
(24) Ying, J. W.; Cordova, A.; Ren, T. Y.; Xu, G. L.; Ren, T. *Chem.—Eur. J.* **2007**, *13*, 6874−6882.
(25) Lin, C.; Ren, T.; J. Valente, E.; D. Zubkowski, J. *J. Chem. Soc., Dalton Trans.* **1998**, 571−576.
(26) Ying, J. W.; Ren, T. *J. Organomet. Chem.* **2006**, *691*, 4021−4027.
(27) Liu, I. P. C.; Ren, T. *Inorg. Chem.* **2009**, *48*, 5608−5610.
(28) Whittall, I. R.; Humphrey, M. G.; Hockless, D. C. R. *Aust. J. Chem.* **1997**, *50*, 991−998.
(29) Whittall, I. R.; Humphrey, M. G.; Hockless, D. C. R. *Aust. J. Chem.* **1998**, *51*, 219−228.
(30) Montalvo-Gonzalez, R.; Ariza-Castolo, A. *J. Mol. Struct.* **2003**, *655*, 375−389.
(31) Xi, B.; Xu, G. L.; Fanwick, P. E.; Ren, T. *Organometallics* **2009**, *28*, 2338−2341.
(32) Ying, J. W.; Sobransingh, D. R.; Xu, G. L.; Kaifer, A. E.; Ren, T. *Chem. Commun.* **2005**, 357−359.
(33) Ying, J. W.; Ren, T. *J. Organomet. Chem.* **2008**, *693*, 1449−1454.
(34) Hansch, C.; Leo, A.; Taft, R. W. *Chem. Rev.* **1991**, *91*, 165−195.
(35) Ren, T. *Coord. Chem. Rev.* **1998**, *175*, 43−58.
(36) Shaabani, B.; Shaghaghi, Z. *Tetrahedron* **2010**, *66*, 3259−3264.
(37) Costuas, K.; Paul, F.; Toupet, L.; Halet, J.-F.; Lapinte, C. *Organometallics* **2004**, *23*, 2053−2068. Paul, F.; Ellis, B. G.; Bruce, M. I.; Toupet, L.; Roisnel, T.; Costuas, K.; Halet, J.-F.; Lapinte, C. *Organometallics* **2006**, *25*, 649−665. Paul, F.; Toupet, L.; Thepot, J. Y.; Costuas, K.; Halet, J. F.; Lapinte, C. *Organometallics* **2005**, *24*, 5464−5478. Denis, R.; Toupet, L.; Paul, F.; Lapinte, C. *Organometallics* **2000**, *19*, 4240−4251.
(38) Xu, G.-L.; DeRosa, M. C.; Crutchley, R. J.; Ren, T. *J. Am. Chem. Soc.* **2004**, *126*, 3728−3729.
(39) Forrest, W. P.; Cao, Z.; Fanwick, P. E.; Hassell, K. M.; Ren, T. *Organometallics* **2011**, *30*, 2075−2078.
(40) Becke, A. D. *J. Chem. Phys.* **1993**, *98*, 5648−5652. Lee, C. T.; Yang, W. T.; Parr, R. G. *Phys. Rev. B.* **1988**, *37*, 785−789.
(41) Stephens, P. J.; Devlin, F. J.; Chabalowski, C. F.; Frisch, M. J. *J. Phys. Chem.* **1994**, *98*, 11623−11627.
(42) Frisch, M. J.; Trucks, G. W.; Schlegel, H. B.; Scuseria, G. E.; Robb, M. A.; Cheeseman, J. R.; Montgomery, J. A., Jr.; Vreven, T.; Kudin, K. N.; Burant, J. C.; Millam, J. M.; Iyengar, S. S.; Tomasi, J.; Barone, V.; Mennucci, B.; Cossi, M.; Scalmani, G.; Rega, N.; Petersson, G. A.; Nakatsuji, H.; Hada, M.; Ehara, M.; Toyota, K.; Fukuda, R.; Hasegawa, J.; Ishida, M.; Nakajima, T.; Honda, Y.; Kitao, O.; Nakai, H.; Klene, M.; Li, X.; Knox, J. E.; Hratchian, H. P.; Cross, J. B.; Bakken, V.; Adamo, C.; Jaramillo, J.; Gomperts, R.; Stratmann, R. E.; Yazyev, O.; Austin, A. J.; Cammi, R.; Pomelli, C.; Ochterski, J. W.; Ayala, P. Y.; Morokuma, K.; Voth, G. A.; Salvador, P.; Dannenberg, J. J.; Zakrzewski, V. G.; Dapprich, S.; Daniels, A. D.; Strain, M. C.; Farkas, O.; Malick, D. K.; Rabuck, A. D.; Raghavachari, K.; Foresman, J. B.; Ortiz, J. V.; Cui, Q.; Baboul, A. G.; Clifford, S.; Cioslowski, J.; Stefanov, B. B.; Liu, G.; Liashenko, A.; Piskorz, P.; Komaromi, I.; Martin, R. L.; Fox, D. J.; Keith, T.; Al-Laham, M. A.; Peng, C. Y.; Nanayakkara, A.; Challacombe, M.; Gill, P. M. W.; Johnson, B.; Chen, W.; Wong, M. W.; Gonzalez, C.; Pople, J. A. *Gaussian 03, Revision D.02*, Wallingford, Ct., 2003.
(43) Hehre, W. J.; Ditchfield, R.; Pople, J. A. *J. Chem. Phys.* **1972**, *56*, 2257−2261. Krishnan, R.; Binkley, J. S.; Seeger, R.; Pople, J. A. *J. Chem. Phys.* **1980**, *72*, 650−654. Hariharan, P. C.; Pople, J. A. *Theor. Chim. Acta* **1973**, *28*, 213−222.
(44) Bunting, P.; Chisholm, M. H.; Gallucci, J. C.; Lear, B. J. *J. Am. Chem. Soc.* **2011**, *133*, 5873−5881. Chisholm, M. H.; Lear, B. J. *Chem. Soc. Rev.* **2011**, *40*, 5254−5265.
(45) Beurskens, P. T.; Beurskens, G.; deGelder, R.; Garcia-Granda, S.; Gould, R. O.; Smits, J. M. M. *The DIRDIF2008 Program System, Crystallography Laboratory*; University of Nijmegen: The Netherlands: 2008.
(46) Sheldrick, G. M. *Acta Crystallogr.. A.* **2008**, *64*, 112−122.
(47) Parr, R. G.; Yang, W. *Density Functional Theory of Atoms and Molecules*; Oxford University Press: New York, 1989.
(48) Hay, P. J.; Wadt, W. R. *J. Chem. Phys.* **1985**, *82*, 270−283. Wadt, W. R.; Hay, P. J. *J. Chem. Phys.* **1985**, *82*, 284−298. Hay, P. J.; Wadt, W. R. *J. Chem. Phys.* **1985**, *82*, 299−310.